THE NATURE OF THE LOW-LUMINOSITY ACTIVE GALACTIC NUCLEI IN NGC 3147

A. PTAK,[1] T. YAQOOB,[2] AND P. J. SERLEMITSOS
NASA/Goddard Space Flight Center, Greenbelt, MD 20771

AND

H. KUNIEDA AND Y. TERASHIMA
Department of Astrophysics, Nagoya University, Chikusa-ku, Nagoya 464-01, Japan

ABSTRACT

A recent optical study has identified an active nucleus (AGN) in the spiral galaxy NGC 3147 based on the discovery of broad (FWHM ~ 400 km s^{-1}) [N II] line emission. This object was previously mis-classified as a normal galaxy. Here we present the first X-ray spectrum obtained by *ASCA* in the 0.4–10 keV bandpass of this source. The X-ray spectrum is typical of Seyfert 1 galaxies, namely, it has little intrinsic absorption, a power-law continuum with a photon index of 1.80 ± 0.09, and Fe Kα emission at around 6.4 keV (rest frame) with an equivalent width greater than 130 eV. However, if it really is a Seyfert 1 galaxy, at a 2–10 keV luminosity of $\sim 5 \times 10^{41}$ ergs s^{-1}, it should be highly variable, in keeping with the established trend that the lowest luminosity AGNs exhibit the greatest variability. However, no variability is observed within the 50 ks *ASCA* observation or between the *ASCA* observation and a *ROSAT* observation 2 weeks later. Alternatively, NGC 3147 may harbor an obscured AGN in which the observed X-ray spectrum is seen only in scattered light and the intrinsic X-ray luminosity may be an order of magnitude or two higher than observed. This interpretation would be consistent with a Seyfert 2 galaxy in the unified Seyfert model. We discuss the physical and geometrical constraints on the obscuring matter and the scattering zone in such a scenario. We point out the contrast with the X-ray spectrum of other Seyfert 2 galaxies which contain a soft, possibly thermal, component not present in NGC 3147.

Subject headings: galaxies: active — galaxies: individual (NGC 3147) — X-rays: galaxies

1. INTRODUCTION

A recent survey of infrared- and X-ray–selected galaxies (based on the *ROSAT* All-Sky Survey [RASS]; Boller et al. 1992) suggests that there may be a class of "normal" spiral galaxies with X-ray luminosities (L_X) of 10^{42}–10^{43} ergs s^{-1}, well in excess of the $L_X \sim 10^{39}$–10^{40} ergs s^{-1} previously seen in infrared-selected normal galaxies (Green, Anderson, & Ward 1992). Boller et al. (1992) suggest that the source of this X-ray luminosity may be starburst activity, presumably dominated by many high-mass X-ray binaries with $L_X \sim 10^{38}$–10^{39} (Griffiths & Padovani 1990). Moran, Halpern, & Helfand (1994) carried out a follow-up study to the Boller et al. (1992) results and found that many of these X-ray luminous sources were in fact low-luminosity AGNs based on previously undetected broad lines in their optical nuclear spectra. Evidence that the bulk of the X-ray emission in spiral galaxies previously classified as "normal" or "starburst" is due to a low-luminosity AGN is becoming increasingly commonplace (e.g., Makishima 1994 and references therein; Dahlem, Heckman, & Fabbiano 1995; Yaqoob et al. 1995). Very little X-ray spectral information exists for such objects above ~ 2 keV because of the limited sensitivity of X-ray detectors prior to *ASCA*. Study of their broadband X-ray spectral properties and comparison with the large body of knowledge of their higher luminosity counterparts, classical Seyfert 1 and 2 galaxies, is important because it can directly impact our understanding of AGN unification and the origin of the X-ray background (cf., Yaqoob et al. 1995 and references therein). Here we present the results of an *ASCA* observation of one of the sources in the Moran et al. (1994) study, NGC 3147, now classified as a Seyfert 2, at a distance of 56 Mpc ($z = 0.0094$; $H_0 = 50$ km s^{-1} Mpc^{-1} and $q_0 = 0$ throughout this paper). Although *HEAO 1* detected emission in the vicinity of NGC 3147 at the ~ 3 σ level (Rephaeli, Gruber, & Persic 1995) and NGC 3147 was detected in the RASS, it was not detected significantly with the *Einstein* satellite (Rephaeli et al. 1995). This *ASCA* observation yields the first X-ray spectral data for NGC 3147 in the 0.4–10 keV bandpass, permitting detailed study of its hard continuum and search for spectral features.

2. *ASCA* DATA

NGC 3147 was observed by *ASCA* in 1993 September 30. See Tanaka, Inoue, & Holt (1994) for a description of the *ASCA* mission and focal plane detectors. Hereafter, we refer to the two ~ 0.4–10.0 keV SIS detectors as S0 and S1 and the two ~ 0.7–10 keV GIS detectors as S2 and S3. The observation was made with the SIS in 4 CCD mode. The data were cleaned in the manner described in Serlemitsos et al. (1994). The spectra were extracted from $\sim 3'$ radius circular regions for the SIS and $6'$ radius regions for the GIS. Background spectra were extracted from annuli with radii $7'$–$12'$, centered on the source for the GIS (analysis of blank sky data shows that vignetting does not significantly impact our determination of the GIS background) and from the remainder of the chip in the SIS (all SIS source counts were extracted from the same chip). The observed count rates were ~ 0.03–0.05 counts s^{-1} with net exposure times of ~ 25–35 ks for the four instruments, the background comprising $\sim 8\%$–10% of the total in SIS and $\sim 28\%$–30% of the total in the GIS. The background was accounted for in

[1] University of Maryland, College Park, MD 20742.
[2] With the Universities Space Research Association.

two ways as a consistency check. First (method 1), we model the background spectra using simple power laws and Gaussians (as required). Second (method 2), we bin the source spectra (to a minimum of 10 counts per channel), allowing use of the χ^2 statistic, and directly subtract the background spectra. Method 1 allows the use of maximum likelihood and does not require binning, preserving the resolution of the data.

3. SPECTRAL FITTING

Table 1 shows the results of fitting the spectra with a simple power law plus cold, uniform absorber. The two methods give consistent results, with the maximum-likelihood fitting preferring a slightly steeper photon index (Γ), by ~ 0.1, and higher column density (N_H) than the χ^2 fitting. Analysis of simulated data shows that this is not a binning effect, and so it must be a reflection of uncertainties in the background subtraction. However, we note that the fit parameters are formally consistent with each other, showing that the details of the background subtraction do not make a significant impact on our results. Since the GIS is not sensitive to $N_H \lesssim 10^{21}$ cm^{-2}, and the best-fitting column densities from fits using the GIS data only were

zero, N_H was set to the Galactic value, 2.5×10^{20} cm^{-2} (Stark et al. 1992), in these fits. The fits using only the SIS data give best-fitting column densities consistent with the Galactic value. Figure 1 shows the power-law (plus cold absorber) four-instrument fit (method 1) with the SIS and GIS data shown separately for clarity. Although the simple model gives an acceptable fit $\chi^2 = 508.9$ (516 degrees of freedom [d.o.f.]), significant residuals are evident between ~ 6–7 keV, indicative of Fe K line emission. Figure 2, in which the data from the four instruments have been combined, shows the Fe K line feature more clearly. This serves to illustrate the significance of the line, and the data combined in this way have not been used in the analysis. Including an additional narrow Gaussian component (intrinsic width fixed at 0.01 keV) with the simple model reduces χ^2 by 13.2 ($\Delta C = 34.4$), which is significant at greater than 99.9% confidence for two additional parameters (the line energy and the line intensity). The results are shown in Table 2 from which it can be seen that the line energy and equivalent width are somewhat dependent on the instruments used in the fits and the method of background subtraction. The four-instrument fit (method 2) gives a line energy consistent with 6.4 keV in the source frame and an equivalent width of 485^{+309}_{-282} eV. The best-fitting line energies for fits using the GIS data only (~ 6.6 keV) are somewhat higher than those using the SIS only (~ 6.4 keV). Although the GIS gain uncertainty can be as much as $\sim 1\%$, another possibility is that there is another spectral feature in addition to an Fe K line at 6.4 keV that is not being resolved by the GIS (the energy resolution is $\sim 8\%$ at 6 keV compared with $\sim 2\%$ for the SIS). Indeed, there are persistent residuals at ~ 7 keV in the power-law plus single line fits. Moreover, if the intrinsic width of the line is allowed to float, it remains comparable to the detector resolution in the SIS fits but increases to ~ 0.4 keV in the GIS fits. When a second narrow Gaussian line component is added to the four-instrument fit, χ^2 is reduced by 7.8 ($\Delta C = 13.2$), which is significant at greater than 98% confidence for two additional parameters. The best-fitting line energy is $7.17^{+0.24}_{-0.30}$ (rest frame) and the

TABLE 1
SIMPLE POWER-LAW FITS TO THE *ASCA* SPECTRA

Detector	Method	N_H ($\times 10^{20}$ cm^{-2})	Γ	χ^2/C (d.o.f.)
S0–S1	1	0.8 (0.0–4.2)	1.66 (1.56–1.78)	2107.4 (690)
S0–S1	2	3.4 (0.0–7.6)	1.74 (1.61–1.89)	194.0 (175)
S2–S3	1	2.5[a]	1.70 (1.62–1.79)	5008.4 (1559)
S2–S3	2	2.5[a]	1.80 (1.69–1.90)	313.2 (340)
S0–S3	1	0.7 (0.0–3.4)	1.66 (1.60–1.75)	7114.9 (2250)
S0–S3	2	3.5 (0.0–7.0)	1.76 (1.66–1.86)	508.9 (516)

NOTE.—Parenthesis give 90% confidence contours for two interesting parameters.

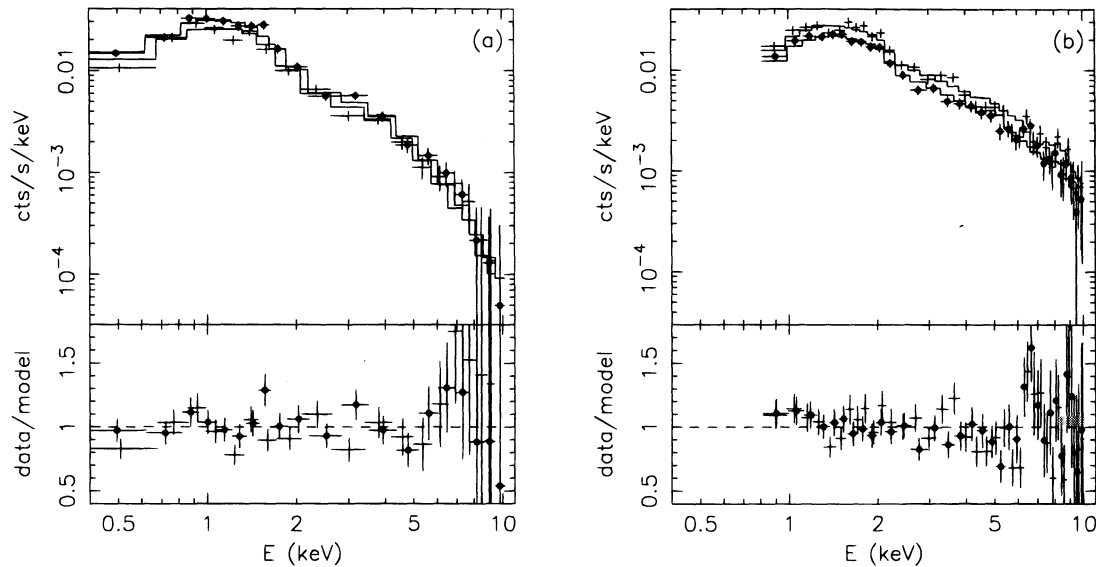[a] Parameter value frozen at this value during fits. See text.

FIG. 1.—Best-fitting power-law model to the data (with the background modeled), with the data binned for display purposes (using "setplot rebin" in XSPEC). SIS data shown in (*a*), with S0 points marked (*filled circles*), and GIS data shown in (*b*), with S2 points marked, for clarity. Note that in this observation the signal-to-noise ratio of the SIS above 5 keV was somewhat poorer than in the GIS due to a lower total efficiency above 5 keV and a shorter net exposure time.

TABLE 2

POWER-LAW PLUS LINE FITS TO THE *ASCA* SPECTRA

Detector	Method	N_H ($\times 10^{20}$ cm^{-2})	Γ	E (keV)	EW (eV)	χ^2/C (d.o.f.)
S0–S1......	1	1.4 (0.0–4.8)	1.69 (1.58–1.82)	6.35 (6.28–6.41)	394 (124–765)	2095.3 (688)
S0–S1......	2	3.8 (0.0–8.1)	1.76 (1.63–1.91)	6.29 (6.03–6.49)	409 (43–818)	188.3 (173)
S2–S3......	1	2.5[a]	1.76 (1.67–1.86)	6.58 (6.42–6.88)	562 (259–946)	4991.4 (1557)
S2–S3......	2	2.5[a]	1.84 (1.74–1.95)	6.59 (6.43–6.96)	700 (286–1082)	298.9 (338)
S0–S3......	1	1.5 (0.0–4.3)	1.71 (1.63–1.80)	6.36 (6.31–6.44)	374 (128–613)	7093.7 (2248)
S0–S3......	2	4.3 (1.6–7.5)	1.80 (1.71–1.89)	6.44 (6.30–6.80)	485 (203–794)	495.7 (514)

NOTE.—Parenthesis give 90% confidence contours for two interesting parameters.

[a] Parameter value frozen at this value during fits. See text.

observed equivalent width is 567^{+439}_{-430} eV. With the addition of the second line, the best-fitting energy of the lower energy line is $6.47^{+0.13}_{-0.14}$ (rest frame) and the observed equivalent width is 480^{+337}_{-318} eV, while the other model parameters are not significantly affected. Bearing in mind that spectral deconvolution of weak sources can be ambiguous, we note that if the second line in the above fits is replaced by an absorption edge at 7.1 keV (due to additional iron, for example), there is no significant reduction in the fit statistic compared to the single-line fits, the 90% confidence upper limit on the optical depth of the edge being ~ 0.3.

We have also tried fitting the spectra with a Raymond-Smith (R-S) model plus a cold absorber; the four-instrument data (method 2) gives an acceptable fit with $\chi^2 = 515$ (515 d.o.f.). Thus the data cannot distinguish between a thermal and nonthermal continuum (although the reduced χ^2 for the thermal model is slightly higher; see Table 1). The best-fitting R-S parameters are $N_H = 0.0^{+1.1}_{-0.0} \times 10^{20}$ cm^{-2}, $kT = 6.03^{+1.08}_{-0.79}$ keV, and an abundance rela-

tive to solar of $0.5^{+0.3}_{-0.3}$. If N_H is forced to the Galactic value, the best-fitting temperature is less by ~ 0.5 keV. There is no significant improvement to χ^2 or the C-statistic when a second continuum component is added to the spectrum, with a solar-abundance R-S decreasing χ^2 by only ~ 2 for two additional degrees of freedom (best-fitting $kT \sim 0.9$ keV). Since the temperature of such a component is not constrained, we fixed the temperature at 0.6 keV (*ASCA* observations of spiral galaxies typically find a soft thermal component with $kT \sim 0.3$–0.6 keV; Makishima 1994) and find that such a component contributes less than 5% of the 0.5–2.0 keV flux. Preliminary analysis of a *ROSAT* PSPC observation of NGC 3147 performed in 1993 October confirms that the data are consistent with a power law with a slope of ~ 1.8 extending down to at least ~ 0.3 keV, with the results of fitting the PSPC spectrum simultaneously with the *ASCA* spectra not differing significantly from the *ASCA* results described above.

Using the power law plus two lines fit described above, the observed mean 2–10 keV flux is $\sim 1.3 \times 10^{-12}$ ergs cm^{-2} s^{-1} ($L_{2-10\,keV} \sim 4.9 \times 10^{41}$ ergs s^{-1}). The four detectors independently give fluxes consistent to within 25% of the mean (the consistency is somewhat poorer than typically seen in *ASCA* observations due to the faintness of the source). The absorption-corrected 0.5–2.0 keV flux is 7.3×10^{-13} ergs cm^{-2} s^{-1}, corresponding to $L_X = 2.7 \times 10^{41}$ ergs s^{-1}. A *ROSAT* PSPC observation of NGC 3147 (see above) obtained a 0.5–2.0 keV flux of $\sim 1.0 \times 10^{-12}$ ergs cm^{-2} s^{-1} (N. Junkes, personal communication), consistent with the *ASCA* flux within the instrumental uncertainties. Note that this 0.5–2.0 keV flux is ~ 50% less than that given in the *ROSAT* All-Sky Survey (Boller et al. 1992), observed between 1990 August and 1991 January. However, fluxes obtained from PSPC data with poor statistics are subject to large uncertainties since the spectral parameters cannot be constrained, and this could easily account for the difference.

We address the question of short-term variability within the *ASCA* observation by combining the S2 and S3 data. Since the SIS data are in 4-CCD mode, in which the source counts fall across chip boundaries and gaps, it is not well suited to study short-term variability for a source as weak as this. Fitting the combined S2 and S3 (background-subtracted) light curves with a constant model gives a χ^2 of 22.2 for 32 d.o.f. Still, the statistics are limited. Although the net exposure of the GIS was ~ 36 ks, the total on-time spanned ~ 50 ks. If we split the observation into just two parts, we obtain S2 + S3 count rates of $8.68 \pm 0.25 \times 10^{-2}$ counts s^{-1} and $9.02 \pm 0.30 \times 10^{-2}$ counts s^{-1}, in the initial and
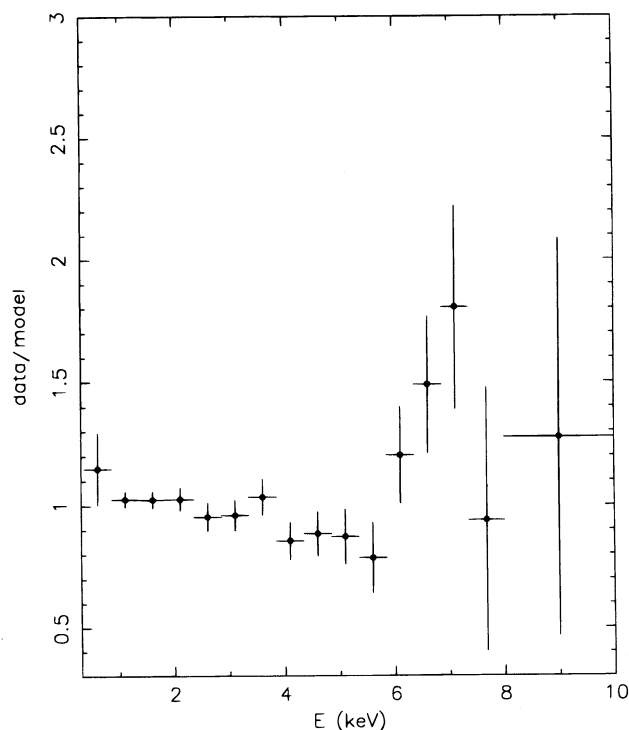

FIG. 2.—Ratio of data to best-fitting power-law model (as in lower panels of Fig. 1) with the data from the four instruments combined. This serves to illustrate the significance of the line, and the data combined in this way have not been used in the analysis.
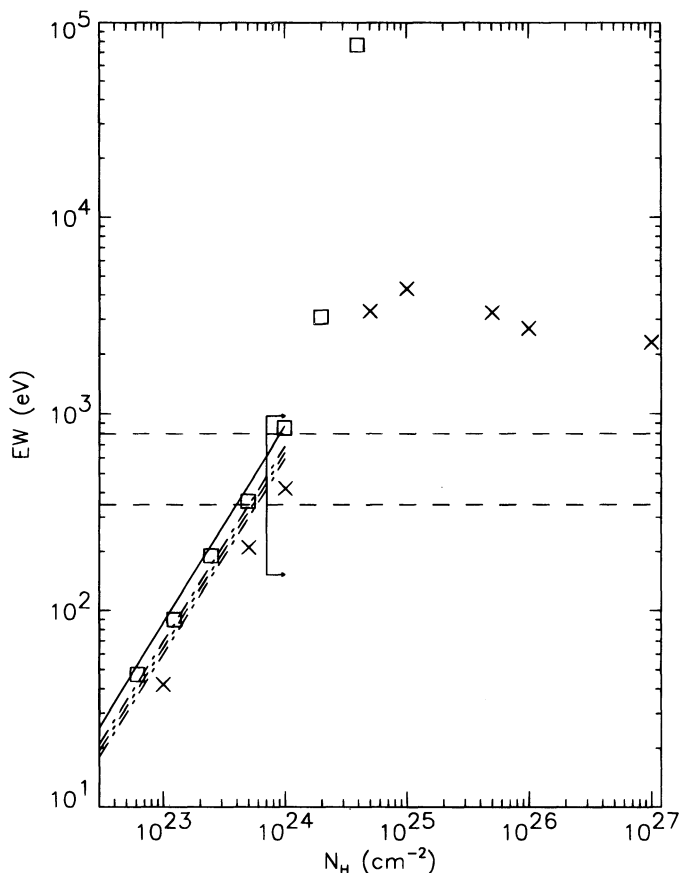
FIG. 3.—Fe-Kα equivalent width (EW) as a function of N_H for various geometries (all assume an isotropic central source). The results of Monte Carlo simulations by Awaki et al. (1991), Leahy & Creighton (1993; LC), and Ghisellini et al. (1994; GHM) are displayed as a solid line, boxes, and crosses, respectively. GHM assume a toroidal geometry and a power-law slope (Γ) of 1.9, while Awaki et al. and LC assume a spherical geometry with $\Gamma = 1.62$ and 1.0, respectively. The models assume a fluorescent yield of 0.34 (corresponding to Fe I), however the models assume different absolute Fe abundances and Fe K edge threshold cross sections. Also shown are the theoretical predictions of Krolik & Kallman (1987; KK) for a spherical geometry (shown as dot-dashed lines) for $\Gamma = 1.6$, 1.8, 2.0, with EW decreasing with increasing Γ), valid for small Thompson depths (i.e., $N_H \lesssim 10^{24}$ cm^{-2}). All models predict a power-law EW–N_H relation (with a slope of ~ 1) for $N_H \lesssim 10^{24}$ cm^{-2}. For this range in N_H, all simulation results agree with the KK prediction (adjusted for the differences in atomic physics assumed by the models) to within 10%. For $N_H \gtrsim 10^{24}$ cm^{-2}, the LC results show a rapid increase in EW with N_H, whereas the GHM show a turn-over followed by a saturation in EW as Compton reflection from the visible portions of the inner surface of the torus dominates transmission through the torus. The allowed range in EW from the NGC 3147 data is marked, with arrows indicating the lower limit for N_H. Finally, the dashed lines show the prediction in KK for the EW resulting from a scattering region (i.e. valid for infinite N_H along the line of sight) in the limits of a cold (EW ~ 800 eV) and a highly ionized (EW ~ 350 eV) scattering medium.

final 25 ks of the observation. Thus we find no evidence for variability within the *ASCA* observation.

4. DISCUSSION

We have shown that the X-ray spectrum of NGC 3147 is indeed consistent with its interpretation in terms of an AGN origin. The 0.4–10 keV spectrum can be characterized by a single power-law continuum with photon index $\Gamma \sim 1.8$ plus at least one emission-line component, corresponding to Fe K emission at ~ 6.4 keV, with an equivalent width of ~ 450 eV (but could be as small as ~ 130 eV and as large as ~ 800 eV). The X-ray spectrum immediately rules

out a dominant contribution from high-mass X-ray binaries (HMXBs) since they have much flatter spectra with $\Gamma \sim 1.0$ (e.g., Nagase 1989). Also, the summed emission from a collection of X-ray binaries may not be able to produce the large equivalent width of the iron line (e.g., Kallman & Krolik 1989). At least $\sim 10^3$ sources would be required since their luminosities are typically less than 10^{38} ergs^{-1}. Further, if the origin of the X-ray thermal were *predominantly* thermal one would expect the iron line energy to be 6.7 keV or higher. Also one would observe characteristic low-energy line emission as in NGC 1068 (Ueno et al. 1994) if the metal abundances are not significantly less than solar.

At face value, the X-ray spectrum of NGC 3147, with its canonical power-law index and Fe K emission line, is typical of a Seyfert 1 galaxy (see, e.g., Nandra & Pounds 1994). However, there are two problems with the interpretation that the AGN in NGC 3147 is simply a Seyfert 1 galaxy at the low-luminosity end of the AGN luminosity function. First, there is a large body of evidence that supports the notion that lower luminosity AGNs are much more variable than high-luminosity AGNs (e.g., see Turner & Pounds 1989; Lawrence & Papdakis 1993; Nandra & Pounds 1994). Seyfert 1 galaxies with 2–10 keV luminosities of the order 10^{42} ergs^{-1} or less generally exhibit rapid large amplitude variability, a factor 2–3 in hundreds of seconds not being uncommon (e.g., NGC 4051; Matsuoka et al. 1990; Mihara et al. 1994). Now the luminosity of NGC 3147 is comparable to NGC 4051, yet we have found no evidence for long- or short-term variability. Even aside from the variability problem, the true equivalent width of the Fe K line would have to be on the smaller side of ~ 500 eV since larger values are difficult to produce with any model in which the line of sight is unobscured and the X-ray source is isotropic. If NGC 3147 is a Seyfert 1 galaxy, an Fe K line of ~ 150 eV EW could be produced by a cold X-ray illuminated accretion disk with standard assumptions (e.g., George & Fabian 1991) and up to ~ 400 eV if the disk is ionized (e.g., Matt, Fabian, & Ross 1993). The parameter space of such a photoionized disk line is very specific but unfortunately the data are not sensitive enough to constrain models further. In the unified scheme of AGNs (e.g., Antonucci & Miller 1985; Lawrence 1987), Seyfert 1 galaxies are thought to correspond to objects in which an obscuring torus is viewed close to its axis, the line of sight being clear. Such a torus could contribute a further ~ 100 eV to the Fe K line (e.g., Krolik, Madau, & Zycki 1994; Ghisellini, Haardt, & Matt 1994), depending on the geometry and Thompson depth.

Given the problems with the interpretation of NGC 3147 as a Seyfert 1 galaxy, an alternative is that the direct emission is heavily obscured and the observed X-ray spectrum is dominated by source photons which have been scattered into our line of sight by an optically thin electron scattering region (which may be photoionized). This is assumed to be the case for Seyfert 2 galaxies in the unified Seyfert model, in which both the obscuring matter (the torus) and the scattering region are key ingredients. Both are expected to be extended on a ~ 1 pc scale so the scattered continuum emission is not expected to vary on timescales less than several years. In this scenario, if the obscuring structure subtends a solid angle $4\pi f$ at the source (assumed to emit isotropically) and the observed luminosity, L_x^{obs} is dominated by the scattered component, then the intrinsic luminosity of the source is $L_x^{intr} \sim L_x^{obs} [(1 - f)\tau_{es}]^{-1}$ (note that as f tends to 1, L_x^{obs}

may be further modified by an anisotropic scattering factor of 3/4 to 3/2). Here, τ_{es} is the Thompson depth of the scattering region, and the unified scheme requires that $\tau_{es} \ll 1$, or else the X-ray spectra of Seyfert 1 galaxies would be modified by transmission in a Compton-thick medium. With the simple condition that the scattered fraction is less than 1 (equivalent to the assumption of an isotropic X-ray source), the data require that $N_H > 7 \times 10^{23}$ cm^{-2} in the obscuring material. Likewise, reflection from optically thick material contributes no more than 57% of the flux at 6.4 keV, which is consistent with reflection from the inner surface of a torus with an inclination angle that is slightly larger than its opening angle (cf., Ghisellini et al. 1994), with a smaller reflection component requiring a larger inclination angle (i.e., an edge-on orientation).

If NGC 3147 really is seen only in reflected light, then an Fe K line with a much larger equivalent width than the unobscured case is easy to produce. In general, Fe K line photons will be generated in the scattering region and in the torus; the latter may be seen in both transmission and reflection. In our case the reflection component is not likely to be important. The net equivalent width will then be proportional to the ratio of the sum of the line intensities to the sum of the continua (discussed above) at the line center energy. Now, in the limit in which the observed continuum is due only to the scattered component (infinite N_H and an edge-on torus), the EW due to the line from the scattering region reaches an asymptotic upper limit which is *independent of the opening angle of the torus* and depends only on Γ and the mean fluorescence yield and abundance of iron in the scattering zone (see Krolik & Kallman 1987). The value of this upper limit ranges from ~ 350 eV for H-like Fe (with $E_{K\alpha} = 6.9$ keV) to 800 eV for neutral Fe. A finite column density along with a decreasing opening angle of the torus can then reduce this contribution to the EW to zero, in principle. As for the torus contribution to the line, many authors have calculated the expected EW, often under different assumptions about the geometry and source continuum. Figure 3 shows a comparison of the predicted EW for some of these models as a function of N_H. While they differ in detail (see caption), it is evident that for $N_H \sim 10^{24}$ cm^{-2} all the models predict an EW from the obscuring material

alone of ~ 400–500 eV. Also shown is the expected maximum equivalent width from the scattering zone for cold and highly ionized Fe (as described above), as well as the measurement limits of the EW from the data. The presence of scattered continuum (required by the data in this scenario since a spectrum dominated by Compton reflection from optically thick material would require an unreasonably steep intrinsic $\Gamma \sim 4.8$) would cause the observed EW to decrease from that expected from the torus and asymptotically approach the upper limits for the EW from the scattering region. It can be seen that one can easily account for the Fe K line EW if NGC 3147 is a Seyfert 2 galaxy in the unified scheme. Note that if the Fe K line in Seyfert 1 galaxies is due to fluorescence in an X-ray illuminated accretion disk and the obscured nuclei in Seyfert 2 galaxies are no different than those in Seyfert 1 galaxies, then one should also expect a disk line associated with the scattered continuum (observed periscopically), its EW being ~ 100–150 eV relative to that continuum.

NGC 1068 is another well-known Seyfert 2 galaxy in which the observed X-ray spectrum is thought to be seen only in scattered light due to heavy obscuration of the direct continuum. However, in that case the *ASCA* spectrum is rich in low-energy line features and a complex of iron emission lines, all indicative of a thermal spectrum that has been attributed to star formation (see Ueno et al. 1994). The lack of a soft component in the *ASCA* spectrum of NGC 3147 is thus in contrast to the *ASCA* spectra of NGC 1068. Also note that the nucleus of NGC 3147 is optically weak compared to AGNs with X-ray luminosities comparable to NGC 3147 (Moran et al. 1994). On the other hand, if NGC 3147 is a Seyfert 1 galaxy, then the lack of X-ray variability in NGC 3147 distinguishes it from other low-luminosity Seyfert 1 galaxies.

REFERENCES

Antonucci, R., & Miller, J. 1985, ApJ, 297, 621
Awaki, H., Koyama, K., Inoue, H., & Halpern, J. 1991, PASJ, 43, 195
Boller, T., Meurs, E., Brinkmann, W., Fink, H., Zimmermann, U., & Adorf, H.-M. 1992, A&A, 261, 57
Dahlem, M., Heckman, T., & Fabbiano, G. 1995, ApJ, 442, L49
George, I., & Fabian, A. 1991, MNRAS, 249, 352
Ghisellini, G., Haardt, F., & Matt, G. 1994, MNRAS, 267, 743
Green, P., Anderson, S., & Ward, M. 1992, MNRAS, 254, 30
Griffiths, R., & Padovani, P. 1990, ApJ, 360, 483
Kallman, T., & Krolik, J. 1989, ApJ, 341, 955
Krolik, J., & Kallman, T. 1987, ApJ, 320, L5
Krolik, J., Madau, P., & Zycki, P. 1994, ApJ, 420, L57
Lawrence, A. 1987, PASP, 99, 309
Lawrence, A., & Papdakis, I. 1993, ApJ, 414, L85
Leahy, D., & Creighton, J. 1993, MNRAS, 263, 314
Makishima, K. 1994, in New Horizon in X-Ray Astronomy, ed. F. Makino & T. Ohashi (Tokyo: Universal Academic Press), 171
Matsuoka, M., Piro, L., Yamauchi, M., & Murakami, T. 1990, ApJ, 361, 440

Matt, G., Fabian, A. C., & Ross, R. R. 1993, MNRAS, 262, 179
Mihara, T., Matsuoka, M., Mushotzky, R., Kunieda, H., Otani, C., Miyamoto, S., & Yamauchi, M. 1994, PASJ, 46, L137
Moran, E., Halpern, J., & Helfand, D. 1994, ApJ, 433, L65
Nagase, F. 1989, PASJ, 41, 1
Nandra, K., & Pounds, K. 1994, MNRAS, 268, 405
Rephaeli, Y., Gruber, D., & Persic, M. 1995, A&A, 300, 91
Serlemitsos, P., Yaqoob, T., Ricker, G., Woo, J., Kunieda, H., Terashima, Y., & Iwasawa, K. 1994, PASJ, 46, L43
Stark, A. A., Gammie, C. F., Wilson, R. W., Bally, J., Linke, R., Heiles, C., & Hurwitz, M. 1992, ApJS, 79, 77
Tanaka, Y., Inoue, H., & Holt, S. 1994, PASJ, 46, L37
Turner, T. J., & Pounds, K. A. 1989, MNRAS, 240, 833
Ueno, S., Mushotzky, R., Koyama, K., Iwasawa, K., Awaki, H., & Hayashi, I. 1994, PASJ, 46, L71
Yaqoob, T., Serlemitsos, P., Ptak, A., Mushotzky, R., Kunieda, H., & Terashima, Y. 1995, ApJ, 455, 508